ARTICLE

Photodissociation Dynamics of Dichlorodifluoromethane (CF_2Cl_2) around 235 nm using Time-Sliced Velocity Map Imaging Technology

Rui Mao[a*], Hong Xiao[a], Yu Hu[a], Qun Zhang[b], Yang Chen[b]

a. School of Mathematics and Physics and Chemical Engineering, Changzhou Institute of Technology, Changzhou 213032, China
b. Hefei National Laboratory for Physical Sciences at the Microscale and Department of Chemical Physics, University of Science and Technology of China, Hefei 230026, China

(Dated: Received on December 19, 2018; Accepted on April 28, 2019)

Photodissociation dynamics of dichlorodifluoromethane (CF_2Cl_2) around 235 nm has been studied using the time-sliced velocity map imaging technology in combination with the resonance enhanced multi-photon ionization technology. By measuring the raw images of chlorine atoms which are formed via one-photon dissociation of CF_2Cl_2, the speed and angular distributions can be directly obtained. The speed distribution of excited-state chlorine atoms consists of high translation energy (E_T) and low E_T components, which are related to direct dissociation on $^3Q_0$ state and predissociation on the ground state induced by internal conversion, respectively. The speed distribution of ground-state chlorine atoms also consists of high E_T and low E_T components which are related to predissociation between $^3Q_0$ and $^1Q_1$ states and predissociation on the ground state induced by internal conversion, respectively. Radical dissociation channel is confirmed, nevertheless, secondary dissociation and three-body dissociation channels are excluded.

Key words: Dichlorodifluoromethane, Time-sliced velocity map imaging technology, Internal conversion

I. INTRODUCTION

In recent decades, photodissociation dynamics of chlorofluorocarbons has attracted quite a few scientists' interests in experimental and theoretical research because it is related to protection of the ozone layer [1, 2]. The photodissociation dynamics of simple chlorofluorocarbons, CF_2Cl_2, was studied by several groups during the past years [3–8]. The first report on the photodissociation dynamics of CF_2Cl_2 at 157 and 193 nm was brought by Bersohn and co-workers [3] and they found that the angular distributions of nascent excited-state chlorine atoms (Cl^*) and ground-state chlorine atoms (Cl) are isotropic. Apart from that, White and co-workers [4] suggested that the Cl^* and Cl products were mostly formed via the following dissociation channel on the photodissociation dynamics of CF_2Cl_2 at 187, 125, and 118 nm:

$$CF_2Cl_2 + h\nu \rightarrow CF_2 + Cl/Cl^* + Cl/Cl^* \qquad (1)$$

However, Baum and Huber [5] investigated the photodissociation dynamics of CF_2Cl_2 at 193 nm and proposed that the Cl^* and Cl products were formed via the following dissociation channel:

$$CF_2Cl_2 + h\nu \rightarrow CF_2Cl + Cl/Cl^* \qquad (2)$$

Kawasaki and co-workers [6] used the velocity map imaging (VMI) technology to study the photodissociation dynamics of CF_2Cl_2 in spectral range of 205–209 nm, and reported that the rupture of C–Cl bond was related to parallel transitions. Takahashi and co-workers [7] also supported dissociation channel (2) by measuring the quantum yields for Cl^* and Cl products at 193 nm. Poterya and co-workers [8] investigated the photodissociation dynamics of CF_2Cl_2 in argon clusters by means of VMI in order to explore the dissociation process for the slow Cl^* and Cl products.

Above all, various studies have been carried out on the photodissociation dynamics of CF_2Cl_2, and the suggested dissociation mechanisms are varied, however, the photodissociation dynamics around 235 nm remains unexplored. Here, we present a study on CF_2Cl_2 by means of time-sliced VMI [9–14], in hope to shed some light on its mechanism. The Cl and Cl^* atoms are probed using a (2+1) resonance enhanced multi-photon ionization (REMPI) scheme, directly acquiring the corresponding speed and angular distributions. Three independent dissociation channels are proposed in the Cl and Cl^* formation, respectively.

*Author to whom correspondence should be addressed. E-mail: maor@czu.cn

II. EXPERIMENTS

The experimental setup has been described in previous studies [15, 16]. The whole setup consists of source chamber, ionization chamber, and detection chamber. The source chamber and ionization chamber are connected with the skimmer to form vacuum differential pumping system. The CF_2Cl_2 gases were mixed with helium (∼95%) at backing pressure of ∼2 atm and expanded through a pulsed nozzle (General Valve Series 9, 0.5 mm orifice). The molecular beam passed through the skimmer into the ion optics which are installed in the ionization chamber, and was intersected at right angles by the dissociation photons in the ion optics. The vertically polarized dissociation laser radiation around 235 nm was derived from the output of an Nd:YAG (GCR-170, Spectra Physics) pumped by a frequency doubled dye laser (PrecisionScan, Sirah) and was focused by an f=210 mm lens. Typical ultraviolet pulse energies were in the range of 150−200 μJ. The pulsed dissociation laser was intersected by the rising edge of pulsed molecular beam to prevent the formation of clusters.

The nascent Cl* and Cl atoms were probed at 235.20 and 235.34 nm via the $4p\,(^2P_{1/2})\leftarrow 3p(^2P_{1/2})$ and $4p\,(^2D_{3/2})\leftarrow 3p(^2P_{3/2})$ (2+1) REMPI schemes. The ions were accelerated in the ion optics and flew through a field-free region. The high-speed ion packet hitted a 40-mm-diameter Chevron-type dual MCPs coupled to a P-47 phosphor screen (APD 3040FM, Burle Electro-Optics). The slice images which were obtained by using a narrow time gate of 60 ns were captured by a charge-coupled device (CCD) camera (Imager Compact QE 1376×1039 pixels, LaVision) and transferred to a computer. The accumulated images were acquired by using an every shot basis for event counting [17]. The electronic signals from the MCP output were amplified with a preamplifier (SR 245, SRS), and then collected by an oscilloscope (TEK 3052B). Time-of-flight spectrum was transferred to a computer by using a General-Purpose Interface Bus (GPIB) interface card (LPCI-3488A) and a Labview program. The raw images were accumulated over 30000 shots or more. The wavelengths, calibrated by a wavemeter, were scanned over a range of 4 cm^{-1} to cover all the speed components of the nascent Cl* and Cl atoms.

III. RESULTS

The slice images of chlorine atoms are shown in FIG. 1. For Cl* atom (FIG. 1(a)), the image shows outer anisotropic distribution and inner isotropic distribution. Whereas, for Cl atom (FIG. 1(b)), the image shows two isotropic distributions. All these features can be coincident with the fact that the speed distributions of Cl* and Cl products can both be fitted with two Gaussian components (FIG. 2). The total translational

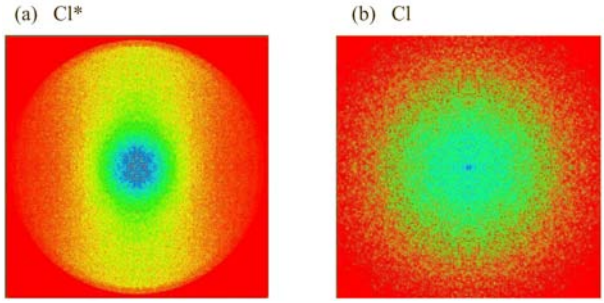

FIG. 1 Slice images of (a) Cl* and (b) Cl atoms for the photodissociation of CF_2Cl_2 measured at 235.20 and 235.34 nm, respectively.

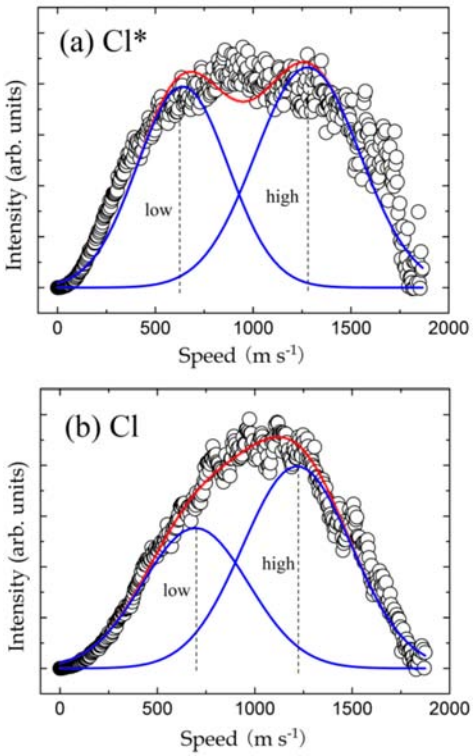

FIG. 2 Speed distributions of (a) Cl* and (b) Cl atoms on the photodissociation of CF_2Cl_2 around 235 nm. Black circles: raw experimental data, blue curves: Gaussian fit to the high and low E_T components, red curve: sums of the fitting distributions.

energy, E_T, can be calculated with the following equation on the assumption that chlorine atoms are formed via dissociation channel (2):

$$E_T = \frac{m_{CF_2Cl_2}}{m_{CF_2Cl}} \times \frac{1}{2} m_{Cl} {v_{Cl}}^2 \qquad (3)$$

where $m_{CF_2Cl_2}$ is the mass of parent molecule CF_2Cl_2, m_{CF_2Cl} is the mass of CF_2Cl radical, m_{Cl} is the mass of chlorine atoms, and v_{Cl} is the speed of chlorine atoms. The internal energy of CF_2Cl radical, E_{int}, can be cal-

DOI:10.1063/1674-0068/cjcp1812283

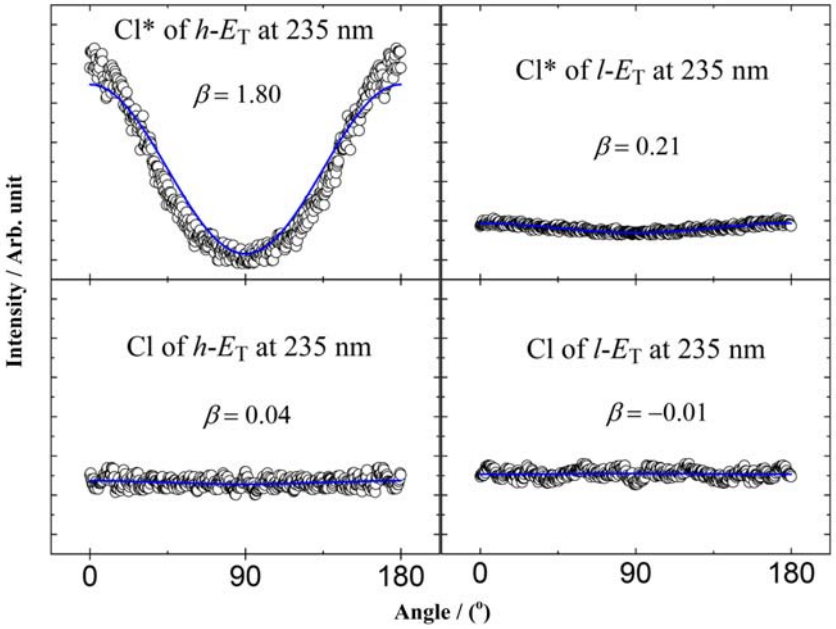

FIG. 3 Angular distributions of chlorine atoms for high E_T and low E_T components on the photodissociation of CF_2Cl_2 around 235 nm. Black circles: raw experimental data, blue curves: the fitting according to Eq.(6).

culated with the following equations:

$$E_{\rm int}\,(CF_2Cl) = h\nu - D_0 - E_T \quad (4)$$

$$E^*_{\rm int}\,(CF_2Cl) = h\nu - D_0 - E_T - E_{\rm so} \quad (5)$$

where $h\nu$ is the energy of one photolysis photon, D_0 is the dissociation energy of the C–Cl bond (348.9 kJ/mol) [6], $E_{\rm int}(CF_2Cl)$ is the internal energy of CF_2Cl radical for Cl atom formation channel, $E^*_{\rm int}(CF_2Cl)$ is the internal energy of CF_2Cl radical for Cl* atom formation channel, and $E_{\rm so}$ is the spin-orbit excitation energy (10.5 kJ/mol) [18]. All these values are shown in Table I.

FIG. 3 shows the angular distributions of chlorine atoms, $I(\theta)$, which can be fitted with the following equation:

$$I\,(\theta) \propto 1 + \beta P_2\,(\cos\theta) \quad (6)$$

where θ is the angle between the photolysis laser polarization and the chlorine atoms recoil velocity, $P_2(\cos\theta)$ is the second-order Legendre polynomial, and β is the anisotropy parameter. For Cl* atoms, the angular distribution for high E_T component was obtained by integrating the speed distribution from 633 m/s to 1868 m/s at each angle, and the angular distribution for low E_T component was obtained by integrating the speed distribution from 0 to 1265 m/s at each angle. For Cl atoms, the angular distribution for high E_T component was obtained by integrating the speed distribution from 700 m/s to 1856 m/s at each angle, and the angular distribution for low E_T component was obtained by integrating the speed distribution from 0 to 1200 m/s at each angle. For Cl* atoms, the values of β for high E_T and low E_T components are 1.80 and 0.21, respectively. For Cl atoms, the values of β for high E_T and low E_T components are 0.04 and −0.01, respectively.

TABLE I Partitions of the available energy and values of β on the photodissociation of CF_2Cl_2 around 235 nm.

Product	$h\nu$/eV	$E_{\rm avl}$/eV	$\langle E_T\rangle$/eV	$\langle E_{\rm int}\rangle/E_{\rm avl}$	β
Cl	508.3	159.4	35.9	0.77	0.04±0.01
			12.0	0.92	–0.01±0.01
Cl*	508.6	149.2	41.4	0.72	1.80±0.01
			9.8	0.93	0.21±0.01

Note: $E_{\rm avl}$ is the available energy, $\langle E_T\rangle$ is the average translational energy, and $\langle E_{\rm int}\rangle$ is the average internal energy. $E_{\rm avl}$ is calculated by using the equations of $E_{\rm avl}(Cl)=h\nu–D_0$ and $E_{\rm avl}(Cl^*)=h\nu–D_0–E_{\rm so}$.

IV. DISCUSSION

The first absorption band of CF_2Cl_2 includes five states $^1Q_2$, $^3Q_1$, $^3Q_0{}^+$, $^3Q_0{}^-$, and $^1Q_1$ as designated by Mulliken [19], and three of which ($^3Q_1$, $^3Q_0{}^+$, and $^1Q_1$) are dissociative electronic states. The $^3Q_1$ and $^1Q_1$ states correlate adiabatically with the formation of Cl atoms via a perpendicular transition, and the $^3Q_0$ state does with the formation of Cl* atoms with a parallel transition character. To clarify the dissociation mechanism more conveniently, a simplified energy diagram of CF_2Cl_2 is shown in FIG. 4, where the $^3Q_1$, $^3Q_0$, and

DOI:10.1063/1674-0068/cjcp1812283

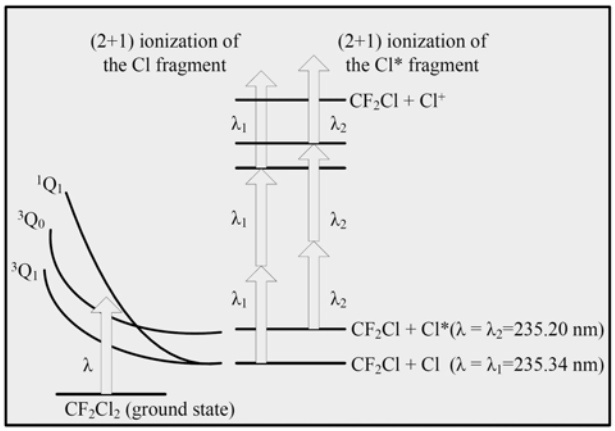

FIG. 4 Schematic potential energy surfaces illustrating the photodissociation of CF_2Cl_2 around 235 nm.

$^1Q_1$ states are in ascending order of excitation energy. In this VMI study, the reaction mechanisms corresponding to high E_T and low E_T components of Cl^* and Cl fragments are discussed as follows, respectively.

A. High E_T component

In the VMI experiments, the dissociation laser radiation around 235 nm is also used to probe Cl^* and Cl atoms via (2+1) REMPI. One photon energy ($h\nu$=508 kJ/mol) is enough to break the C–Cl bond. Furthermore, the high E_T component of Cl^* atoms exhibits a typical parallel transition character. All these features can be ascribed to one-photon photodissociation of CF_2Cl_2 around 235 nm via the following radical channels:

$$CF_2Cl_2 + h\nu_{235.20\ nm} \rightarrow CF_2Cl + Cl\left(^2P_{1/2}\right)$$
$$CF_2Cl_2 + h\nu_{235.34\ nm} \rightarrow CF_2Cl + Cl\left(^2P_{3/2}\right)$$

It is reasonable that the high E_T component of Cl^* product is related to an initial parallel transition from ground state to the $^3Q_0$ state, followed by direct dissociation on $^3Q_0$ state. Such an interpretation is coincident with the fact that the value of β is close to +2.

For high E_T component of Cl product, the value of β is close to 0 (characteristic of predissociation). This can be interpreted as a result of an initial transition from ground state to the $^3Q_0$ state, followed by the nonadiabatic transition from $^3Q_0$ to $^1Q_1$ state. As shown in FIG. 4, the transition from $^3Q_0$ to $^1Q_1$ state has a crossing point. The rate of nonadiabatic transition is probably slowed down as the distance between the excitation position and the crossing point increases in the intersection area. When the rate of the curve crossing is slow, the character of initial parallel transition will be erased. The isotropic high E_T component of Cl atoms is produced in this slow predissociation reaction.

What is noteworthy is that the image on the photodissociation of CF_2Cl_2 around 193 nm shows one sharp ring [8], while the images reported here are rater diffuse. As a matter of fact, the photoabsorption cross section around 193 nm is much larger than that around 235 nm [20]. When the parent molecule absorbs the photon energy around 193 nm, the rupture of C–Cl bond is more prompt than that around 235 nm, so vibrational and rotational excitations of CF_2Cl radical are less sufficient, which is related to the formation of sharp ring.

B. Low E_T component

The low E_T components of Cl^* and Cl atoms exhibit central diffuse distributions as well as isotropic angular distributions. What is the origin of the low E_T components? One possible dissociation channel is the secondary dissociation process:

$$CF_2Cl + h\nu_{235\ nm} \rightarrow CF_2 + Cl\left(^2P_{3/2}\right)/Cl\left(^2P_{1/2}\right)$$

The dissociation energy of this unimolecular decay is about 212 kJ/mol [4–6], so the available energy of 160 kJ/mol (see Table I) is not sufficient.

Another explanation of the low E_T components may be ascribed to the following three-body dissociation channel:

$$CF_2Cl_2 + h\nu_{235\ nm} \rightarrow CF_2 + 2Cl$$

The dissociation energy of this pathway is 552 kJ/mol [6], so the photolysis photon energy of 508 kJ/mol is also not sufficient.

It is to be noted that the slow Cl^* and Cl atoms may be formed on the photodissociation of clusters. The strong central distribution should be clearly observed on the photodissociation of clusters reported by Poterya and co-workers [8], nevertheless, it has not been observed in the present VMI experiments.

In addition, we should also consider the electronic relaxation process, for instance, the internal conversion. Internal conversion is a radiationless de-excitation transition, which is characteristic by isotropic angular distribution and low E_T distribution. The low E_T components of Cl and Cl^* atoms in the present VMI experiments are both isotropic. Based on the above discussion, an internal conversion from the excited state followed by an indirect dissociation on the ground potential energy surface (PES) is suggested. It is reasonable that the well on the ground PES and intramolecular relaxation will reduce the initial alignment and increase the vibration and rotation excitations. This is concident with the fact that the value of β is smaller than that of direct dissociation. For low E_T components of Cl and Cl^* atoms, the values of $\langle E_{int}\rangle/E_{avl}$ (E_{avl} denotes the available energy) are obviously higher than that of direct dissociation (see Table I). The same mechanism was also found in CF_2BrCl [21] and CH_2BrCH_2Cl [22].

DOI:10.1063/1674-0068/cjcp1812283

To summarize, the relevant energy levels are shown schematically in FIG. 4 to illustrate the reaction mechanism of CF_2Cl_2 and the (2+1) REMPI of Cl and Cl^* fragments around 235 nm. Radical dissociation channel is confirmed, nevertheless, secondary dissociation and three-body dissociation channels are excluded.

V. CONCLUSION

We have explored the photodissociation dynamics of CF_2Cl_2 around 235 nm using the time-sliced VMI technology. The nascent Cl and Cl^* atoms are produced via one-photon dissociation and (2+1) REMPI process. The high E_T components of Cl^* fragments are produced via the prompt dissociation on $^3Q_0$ excited PES, nevertheless, the high E_T components of Cl fragments are related to predissociation on $^1Q_1$ excited PES by nonadiabatic $^1Q_1 \leftarrow ^3Q_0$ transition. The low E_T components of Cl and Cl^* fragments are produced via internal conversion.

VI. ACKNOWLEDGMENTS

This work was supported by the Natural Science Foundation of the Jiangsu Higher Education Institutions of China (No.17KJB150005 and No.17KJD510001), the Natural Science Foundation of Changzhou Institute of Technology (No.YN1507 and No.YN1611), Undergraduate Training Program for Innovation of Changzhou Institute of Technology (No.2017276Y), and the National Natural Science Foundation of China (No.21273212).

[1] M. J. Molina and F. S. Rowland, Nature (London) **249**, 810 (1974).
[2] F. S. Rowland and M. J. Molina, Rev. Geophys. Space Phys. **13**, 1 (1975).
[3] Y. Matsumi, K. Tonokura, M. Kawasaki, G. Inoue, S. Satyapal, and R. Bersohn, J. Chem. Phys. **94**, 2669 (1991).
[4] M. Yen, P. M. Johnson, and M. G. White, J. Chem. Phys. **99**, 126 (1993).
[5] G. Baum and J. R. Huber, Chem. Phys. Lett. **203**, 261 (1993).
[6] M. Mashino, H. Yamada, A. Sugita, and M. Kawasaki, J. Photochem. Photobiol. A **176**, 78 (2005).
[7] F. Taketani, K. Takahashi, and Y. Matsumi, J. Phys. Chem. A **109**, 2855 (2005).
[8] V. Poterya, J. Kočišek, A. Pysanenko, and M. Fárník , Phys. Chem. Chem. Phys. 1**6**, 421 (2014).
[9] A. T. J. B. Eppink and D. H. Parker, Rev. Sci. Instrum. **68**, 3477 (1997).
[10] J. J. Lin, J. Zhou, W. Shiu, and K. Liu, Rev. Sci. Instrum. **74**, 2495 (2003).
[11] D. Townsend, M. P. Minitti, and A. G. Suits, Rev. Sci. Instrum. **74**, 2530 (2003).
[12] Y. Liu, G. Knopp, and T. Gerber, Phys. Rev. A **92**, 042501 (2015).
[13] Y. Liu, W. Yin, T. Gerber, F. Jin, and G. Knopp, Laser Phys. Lett. **14**, 105301 (2017).
[14] Y. Yan, Y. Liu, P. Ding, and W. Yin, Acta Phys. Sin. **67**, 203301 (2018).
[15] R. Mao, Q. Zhang, J. Zang, C. He, M. Chen, and Y. Chen, J. Chem. Phys. **135**, 244302 (2011).
[16] R. Mao, C. He, M. Chen, D. Zhou, Q. Zhang, and Y. Chen, Chin. J. Chem. Phys. **30**, 123 (2017).
[17] B. Y. Chang, R. C. Hoetzlein, J. A. Mueller, J. D. Geiser, and P. L. Houston, Rev. Sci. Instrum. **69**, 1665 (1998).
[18] A. Melchior, I. Bar, and S. Rosenwaks, J. Chem. Phys. **107**, 8476 (1997).
[19] R. S. Mulliken, J. Chem. Phys. **3**, 513 (1935).
[20] M. F. Merienne, B. Coquart, and A. Jenouvrier, Planet. Space Sci. **38**, 617 (1990).
[21] J. Huang, D. Xu, J. S. Francisco, and W. M. Jackson, J. Chem. Phys. **119**, 3661 (2003).
[22] L. Hua, H. Shen, C. Zhang, Z. Cao, and B. Zhang, Chem. Phys. Lett. **460**, 50 (2008).

DOI:10.1063/1674-0068/cjcp1812283